CB-NOTE 291 25.10.1996

Acceptance Studies for Analysis of Channels Including Charged Kaons

Christian Völcker
Stefan Spanier

Abstract

We are going to present analyses of final states which include charged kaons. In comparison to pions their hadronic interaction in the CsI(Tl) crystals is more complex and not correctly simulated in the Monte Carlo CBGEANT. We report here our understanding of the kaonic interaction and how to adjust the reconstruction efficiency for the channels $K^+K^-\pi^0$ and $K_LK^\pm\pi^\mp$.

Contents

1 The Hadronic Interaction in the Barrel

We are going to publish data on annihilation channels including charged kaons. Therefore we have to establish the systematics introduced by this particle type very carefully and correct for discrepancies between simulation and reality for our selection criteria.

Two packages are presently on the market to simulate hadronic interactions in the crystals and which are included in the GEANT [1] based CBGEANT program. They can be called optionally. Both fail to describe the K^- . We concentrate on FLUKA here. FLUKA treats the K^- exactly as K^+, if their momentum becomes less than 300 MeV/c. For both charges the hadronic cross section becomes zero in that case. This is a good approximation for K^+, but not for K^-. In reality, the probability for slow or stopped negative kaons to be captured by a nucleon and to form a Λ or Σ resonance is almost 100% . Neither the total nor the inelastic hadronic cross section of kaons is known down to very low kaon energies and the number of possible decay combinations is high. The cross section functions above 300 MeV/c are realistic, but still the subsequent reactions are not correctly included. It needs additional R&D to have a general applicable GEANT. The appearance of K^+ and K^- in the crystals is shown in fig. 1 (the energy in a kaon cluster) and in fig. 2 (the cluster size).

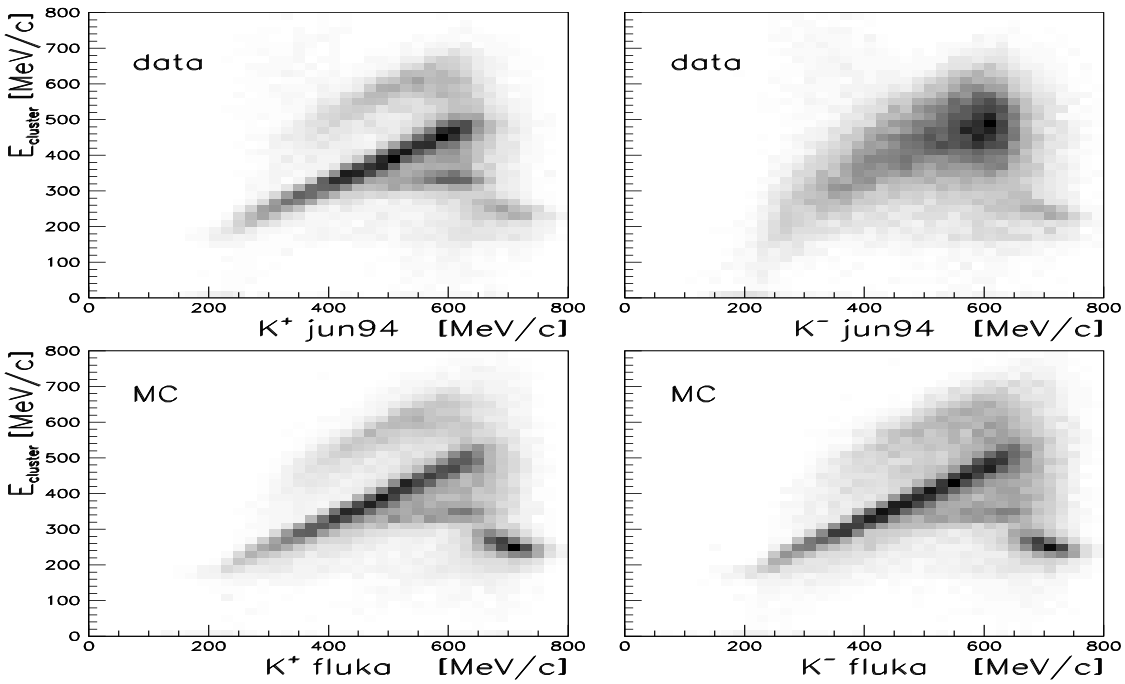

Figure 1: Energy deposit in a cluster formed by K^+ and K^-, compared to the FLUKA simulation.

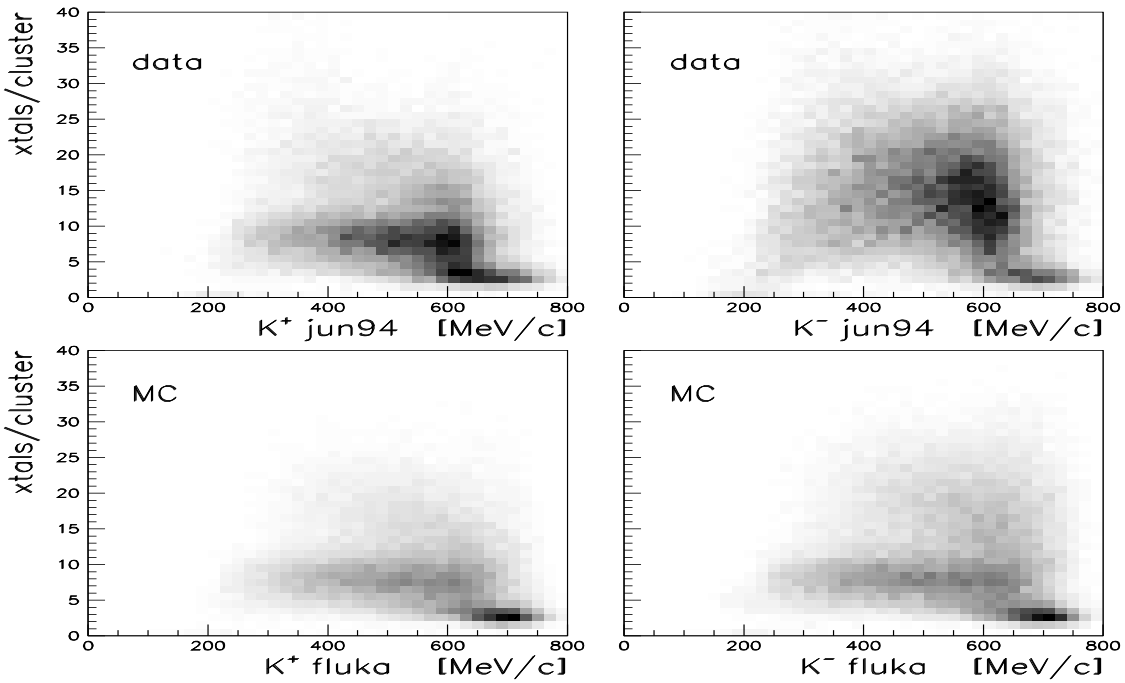

Figure 2: Number of hit crystals in a cluster belonging to K^+ (left) or K^- (right), compared to the FLUKA simulation.

For the CBAR-analyes it depends on the selection criteria (geometrical cuts) how much we are affected by the discrepancies between Monte Carlo and real data. Usually we extrapolate a charged kaon track from the JDC into the barrel and exclude crystals which are matched from a further search of radiative decay products. The following parameters are of interest:

- the cluster location (matching probability),
- the size of the kaonic clusters (decreases the active solid angle for additional real photons)
- the backsplash probability (additional tracks in the JDC)
- the split-off probability (additional PEDs in the barrel)
- the energy deposit.

We will discuss these effects and their possible momentum dependendence in the following sections. We then will establish the corrections to the Monte Carlo efficiency. We start with samples for which we based the selection on the charged tracking.

2 Behaviour of Kaons seen by CBAR

The following momentum dependend behaviour of charged kaons is observed with the Crystal Barrel detector:

initial momentum [MeV/c]	behaviour
$p < 130$	The charged kaons stop in the material before they reach the JDC. They are lost for the detection.
$130 < p < 200$	The kinetic energy of the kaons is too low to reach the crystals (they stay within the JDC or just reach the entrance of the barrel and the decay products encounter for the energy deposit but somewhere else). There is no matching between a PED and the kaon track.
$200 < p < 600$	The kaons are stopped within the crystals. K^+ and K^- can decay into π or μ having a momentum of 230 MeV/c or less. The decay products can travel through several crystals and deposit most of the energy at the end of the trajectory. We expect larger clusters compared to charged pions and secondary PEDs.
$600 < p$	Kaons deposit energy due to ionisation only, except for a few which interact hadronically in flight.

Two features have to be considered in addition:

- If the initial momentum of the kaons is less than 300 MeV/c their energy loss due to ionisation in the target and the surrounding material leads to a correction of the momentum measured with the JDC. The correction function to the transversal momentum is extracted from the Monte Carlo in dependence of the total momentum before the application of the kinematic fit. Figure 3 shows the reconstructed versus the simulated transversal kaon momentum.

- In the K^- -nucleon process Λ's and Σ's are produced. They often decay into

mesons and and a neutron. Interactions of neutrons with nuclei normally hit only one crystal, so most of them are rejected by the definition of a PED. The decay mesons broaden the initial K^- cluster of hit crystals.

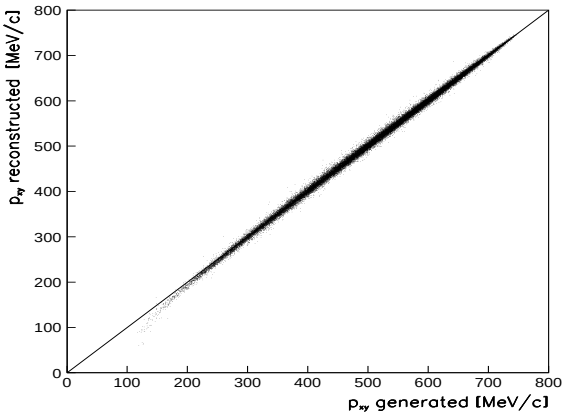

Figure 3:
The transversal momentum of the charged kaon, the reconstructed value versus the simulated value.

3 Data Selection

The parent samples are 1.3 Mio minimum biased annihilations in LH_2 from June 94, 300.000 $K^+K^-\pi^0$ and 400.000 $\pi^+\pi^-\pi^0$ events generated by monte carlo, using GEANT 3.21 and CBGEANT 5.05/00, with the FLUKA package for hadronic interactions.

The software versions for the event reconstruction are

- CBOFF version 1.30/00
- LOCATER version 2.01/00
- BCTRAK version 2.04/00 [1]
- GTRACK version 1.36/00
- CCDBCB version 2.05/00

We prepare least biased samples for the study of the kaon effects in the barrel. The following definitions are applied:

- golden track : first layer 1-3, last layer 21-23,
  number of hits > 10, helix fit $\chi^2 < 1.2$

[1] routine BCEVCK from update to 2.04/01

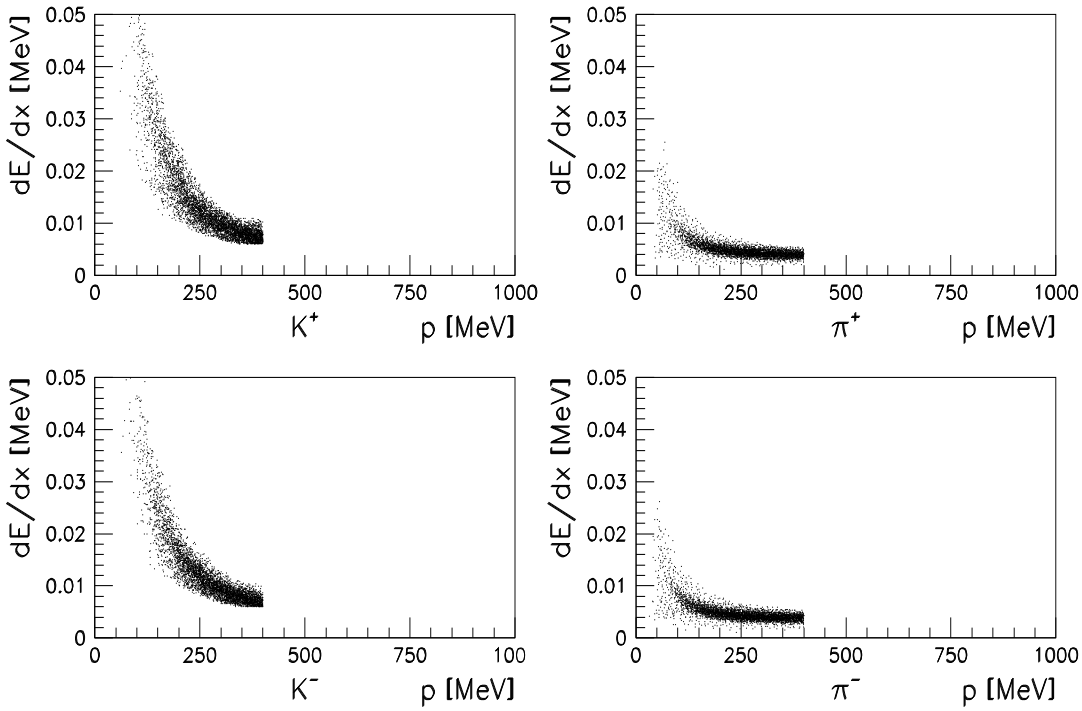

Figure 4: Particle identification using dE/dx for measured particle momenta below 400 MeV/c. The four classifications are shown.

- golden PED : central crystal energy $E1 > 14$ MeV, $E1/E9 < 0.96$ (E9 being the energy in all 9 crystals around the center crystal), no taxi flag set, no dolby-c flag set, ped not in a cluster matched to a charged track

From the parent samples above we select all events with two golden tracks allowing for any additional number of non-golden tracks. We do not specify the number of PEDs at that point. We separate the pionic golden tracks from the kaonic golden tracks using the dE/dx information calculated from at least ten points per track. An at least 1σ separation of kaons from pions is possible for momenta up to 400 MeV/c (see fig. 4). It turns out that the difference of K^+ compared to K^- in the barrel decreases with momentum and becomes very small above 400 MeV/c. We do not expect major new effects at higher momenta causing asymmetries between K^+ and K^- detection.

To examine the momentum dependence of the various aspects, we collect the corresponding parameters in 10 slices of 40 MeV/c width each, covering the range from 0 to 400 MeV/c momentum. For comparison each slice is normalized to the number of events per slice. This eliminates any effect introduced by the dE/dx cuts.

	june 94 min bias	mc fluka $K^+K^-\pi^0$	mc fluka $\pi^+\pi^-\pi^0$
total good events	1312567	300000	400000
events with 2 golden tracks	289228	48199	52412
π^+ golden tracks, $p < 400$ MeV/c	216932	-	43444
π^- golden tracks, $p < 400$ MeV/c	244764	-	47958
K^+ golden tracks, $p < 400$ MeV/c	4787	31129	-
K^- golden tracks, $p < 400$ MeV/c	4579	35004	-

Table 1: Data selection for the acceptance studies.

4 Charged Tracking

The detection for slow kaons may be more efficient than for pions, as kaons produce a stronger ionization signal in a JDC drift cell. The peak number of hits per golden track is 19 for pions but 20 for kaons. At present, there is no method to separate pionic tracks from kaonic tracks before they have been reconstructed. We assume that the charged particles are simulated correctly in the Monte Carlo.

5 Matching Probability

A PED is matched by a charged track in the following way:
An electromagnetic shower direction is assigned to the local energy maximum. The direction of the shower in the barrel must agree with the trajectory of the charged particle within 12 degrees.
This is the case for 95% of all tracks above 400 MeV/c particle momentum. Low momentum charged particles can be stopped in the material between JDC and barrel or may not have enough kinetic energy to create a distinct local maximum in the crystals being stopped there. The decay products of the latter can travel quite far through the CsI-crystals and deposit the major part of energy at the end of their trajectory. This displacement of the energy deposit leaves unmatched PEDs. Such a PED may be counted as golden PED, which is still correlated with the original track. To quantify this we define the matching probability P_{match} as:

$$P_{match} = \frac{n_{match}(p)}{n_{tot}(p)}, \tag{1}$$

where p is the particle momentum, $n_{match}(p)$ the number of matched golden tracks found at momentum p and $n_{tot}(p)$ the total number of golden tracks found at momentum p.

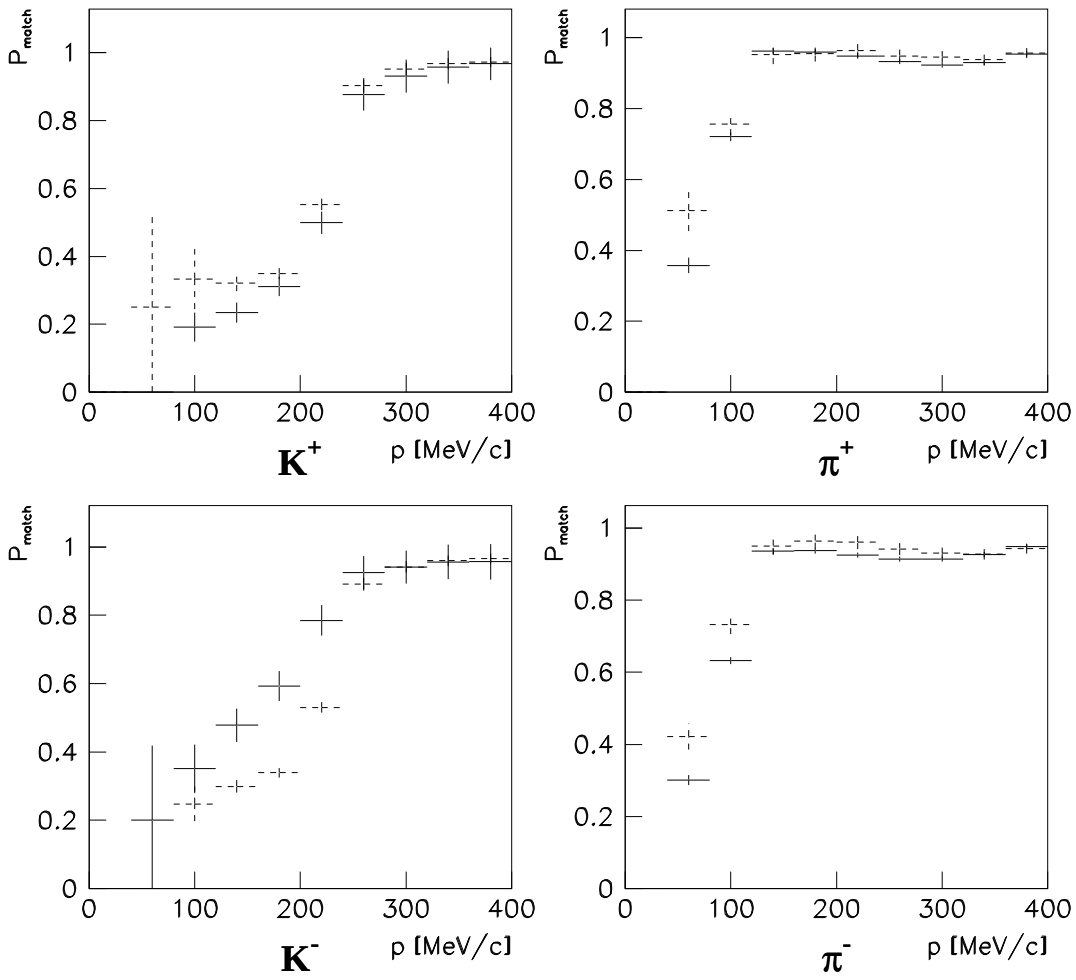

Figure 5: Matching probability for K^+,π^-, K^- and π^-: Real data (solid) and Monte Carlo (dashed)

Figure 5 compares momentum dependence of the matching probability P_{match} for kaons and pions with the Monte Carlo simulation.
The mean number n_{gold} of golden charged split-offs per unmatched track is extracted the following : The distribution of $\cos\theta$ (θ is the opening angle between the PED and the entrance point of the track into the barrel) is in first approximation flat for real photons. In the region between $\cos\theta = -0.5$ and $\cos\theta = 0.7$ it is fit to a constant, which is extrapolated to smaller angles. The excess of events seen in the region $0.7 < \cos\theta < 0.98$ is integrated after the constant has been subtracted. The result of the integration per momentum bin is normalized to the number of unmatched tracks found in the same momentum range (see Fig. 6).

Neglecting the possibility, that more than one golden PED is produced, we

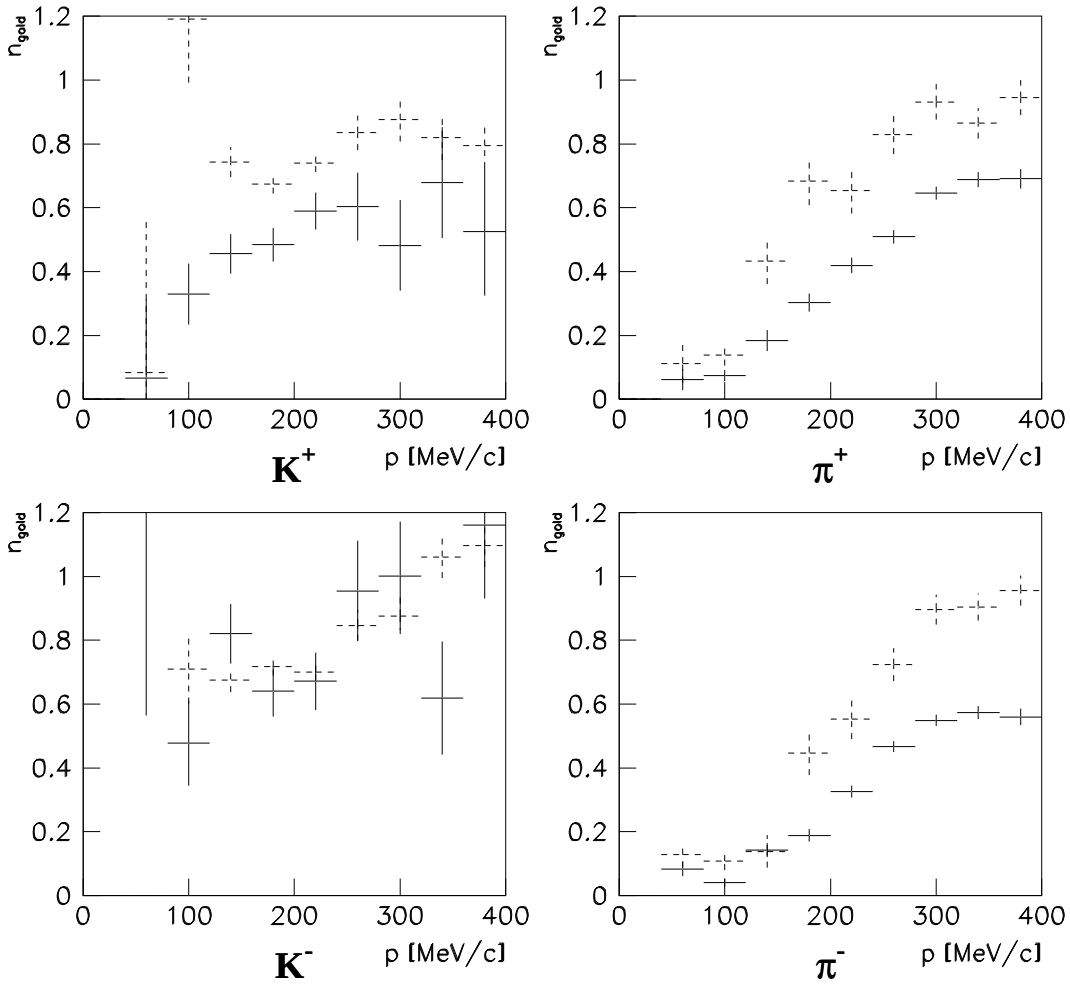

Figure 6: Average number of golden PEDs from unmatched tracks for K^+,π^+, K^- and π^-: Real data (solid) and Monte Carlo (dashed).

arrive at the efficiency ε_{match} induced by the matching algorithm for each particle type :

$$\varepsilon_{match} = 1 - (1 - P_{match}) \cdot n_{gold} \tag{2}$$

The distribution of the efficiency ratio in dependence of the momentum $f_{matchcorr} = \varepsilon_{match(DATA)}/\varepsilon_{match(MC)}$ is the additional acceptance correction function we need. For both, positive and negative pions, $f_{matchcorr}$ turns out to be constant and close to one. For kaons the functions can be parametrized as follows:

$$f^{K^+}_{matchcorr} = 1.1259 + 0.082793 \cdot \arctan[(218.87 - p_{K^+}) \cdot 0.27111] \tag{3}$$

$$f^{K^-}_{matchcorr} = 1 - (0.54259 - 0.0034813 \cdot p_{K^-}) \{0.5 + 0.3183 \cdot \arctan[(225.87 - p_{K^-}) \cdot 0.27111]\} \tag{4}$$

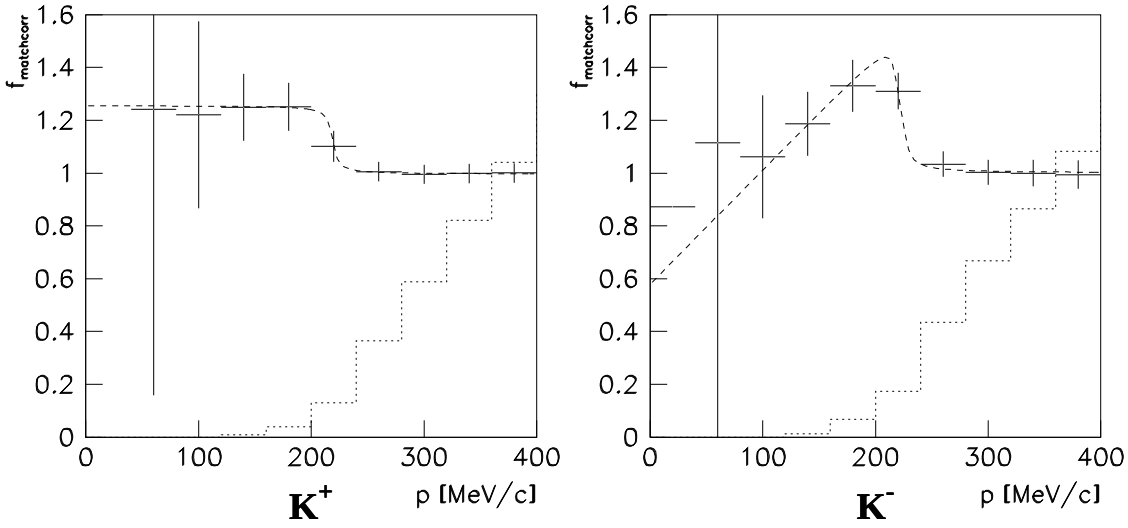

Figure 7: Acceptance correction function $f_{matchcorr}$ for unmatched golden PEDs. dashed line: fitted function; error bars: $\varepsilon_{match,DATA}/\varepsilon_{match,MC}$ fitted, dotted histogam: Monte Carlo momentum spectrum ($K^+K^-\pi^0$)

Figure 7 shows the efficiency ratio $f_{matchcorr}$ for K^+ and K^- versus momentum as extracted from data and Monte Carlo. Also shown is the momentum spectrum of the charged kaons in the channel $\bar{K}K\pi$. Important to notice, that a strong deviation of $f_{matchcorr}$ from 1 appears only below 240 MeV/c kaon momentum. Here K^+ and K^- behave differently. But since the relative population of the $\bar{K}K\pi$ final states goes to zero below 240 MeV/c the mismatching effect plays no dominant role. We will concentrate here on the correction for K^+ only. After correction of our $\bar{K}K\pi$ data for known behaviour of K^+ we will attribute remaining differences in the acceptance between K^+ and K^- to the K^-. This is described in section 9 and 10.

Based on that investigation one can propose a new matching algorithm. Most of the unmatched tracks, although they have no local energy maximum within 12 degrees, leave a signal in the crystal which is hit when entering the barrel. Therefore one should not only try to match the PED's central position but also check if there is such a first crystal which gave a signal above a certain treshold (e.g. 4 MeV). Declare the PED to which the Crystal belongs also as matched.

6 Backsplash Probability

Secondary tracks can be produced from interactions or decay of charged particles in the crystals or material between JDC and barrel. They proceed backwards into the JDC (we call them *backsplash*). Depending on the trigger conditions events containing such secondaries are rejected already on-line. To study the con-

sequences, we distinguish in the definition *backsplashes* and *golden vertex* tracks as follows:

> A *backsplash* is a track whose approach to the origin was not closer then 1.5 cm in r or 2.2 cm in z.
>
> A *golden vertex track* is a golden track which starts in the target region and hence has not been classified as a backsplash.

This backsplash definition includes tracks from secondary vertices outside the target region, such as K_s decays or gamma conversions. These can be avoided if we associate a backsplash always with a true vertex track and proceed analogue to the previous section :

> Histogram the cosine of the opening angle between the extrapolated entrance points in the barrel of the golden vertex track and each backsplash.
>
> Fit the uncorrelated backsplashes as a constant background.
>
> Integrate over the background subtracted signal from $\cos\theta = 0.98$ to $\cos\theta = 1.0$.

We find a negligible fraction of backsplashes for pions, while it is 6 to 7% for kaons. The backsplash probability is 1.5% higher in data than in Monte Carlo for both K^+ and K^-, but momentum independend. It is displayed in fig. 8. The correction will be taken into account in the determination of the reconstruction efficiency (branching ratio).

7 Photon Blindness

We find that for negative kaons the mean cluster size in Monte Carlo is only half of the size seen in real data. This fact has triggered the study on the *photon blindness*. It is defined as the fraction of the barrel's solid angle in which a photon's electromagnetic shower is assigned to a charged particle cluster. It can be flagged as a charged split off PED e.g. by TAXI [2]. If the corresponding PEDs merge the true photon energy cannot be extracted. In both cases the photon (or an interacting K_L) is hidden for the standard reconstruction. Hence, we will establish for each track, how many crystals have been *examined by TAXI*. It turns out (see fig. 9) that Monte Carlo and real data differ up to 20 crystals in cluster size. I.e. the average photon blindness is 1.5% higher in data than in Monte Carlo under the assumption that the photons are distributed uniformly in space. This number is taken into account for the branching ratio of channels with negative kaons.

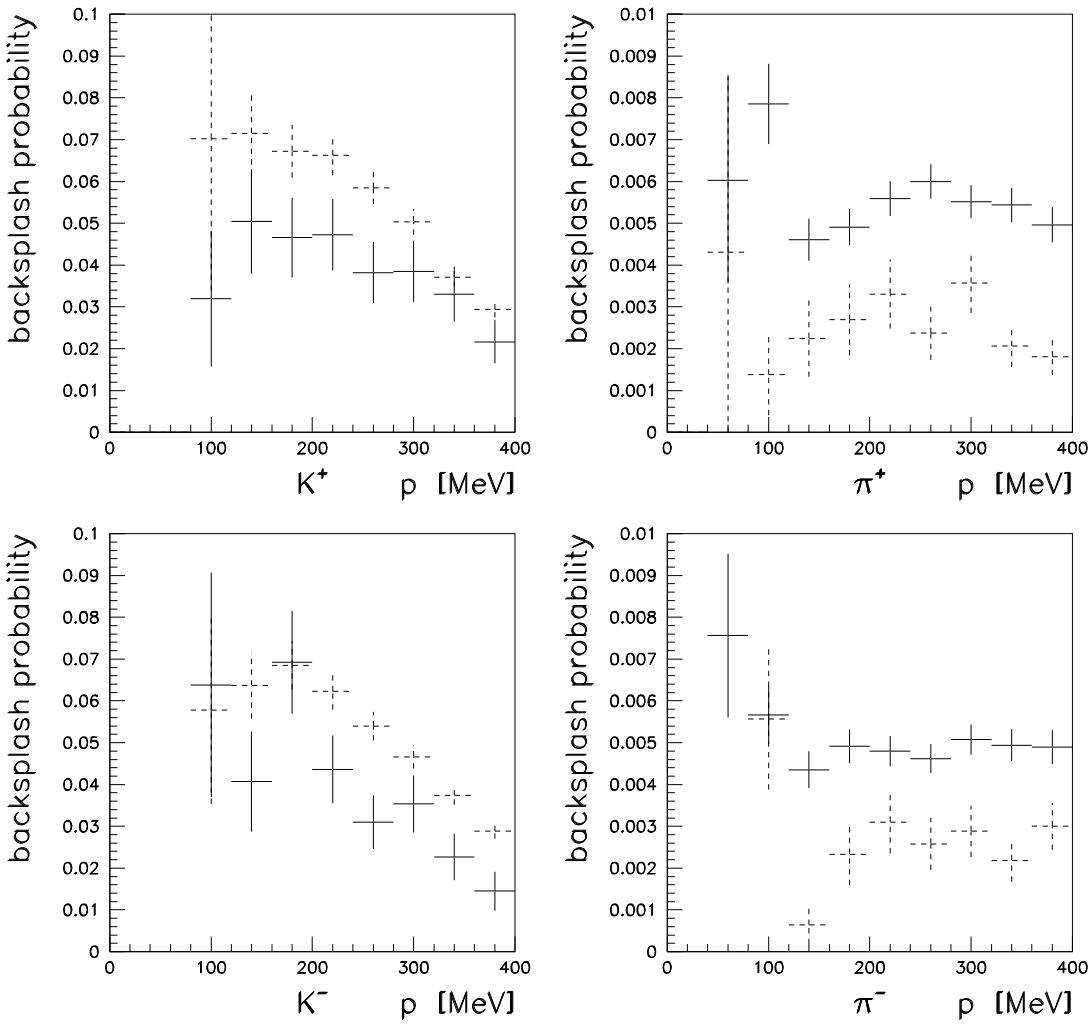

Figure 8: Backsplash probability for K^+, π^+, K^- and π^-. Real data solid, and Monte carlo dashed

The situation in $K^+K^-\pi^0$. If the relative momentum between a charged kaon and the π^0 is very small, i.e. the second kaon has maximum momentum, then the probability of finding a photon from the π^0 decay inside the kaon TAXI cluster increases. Figure 10 (left) compares the opening angle distribution of gammas and kaons for low and high relative momentum in Monte Carlo simulation of $K^+K^-\pi^0$. Fig. 10 (right) displays the Dalitz plot for events that have one gamma within $\cos\theta > 0.7$ opening angle to the K^- track. The affected region is at the left edge of the Dalitz plot where the K^+ momentum is maximal and the π^0 flying almost parallel to the K^-. The described effect accounts for a slight asymmetry in the population of the $K^\star$ band in the bins near the boundary.

The situation in the $K^-K_L\pi^+$ and $K^+K_L\pi^-$ final states: We want to recon-

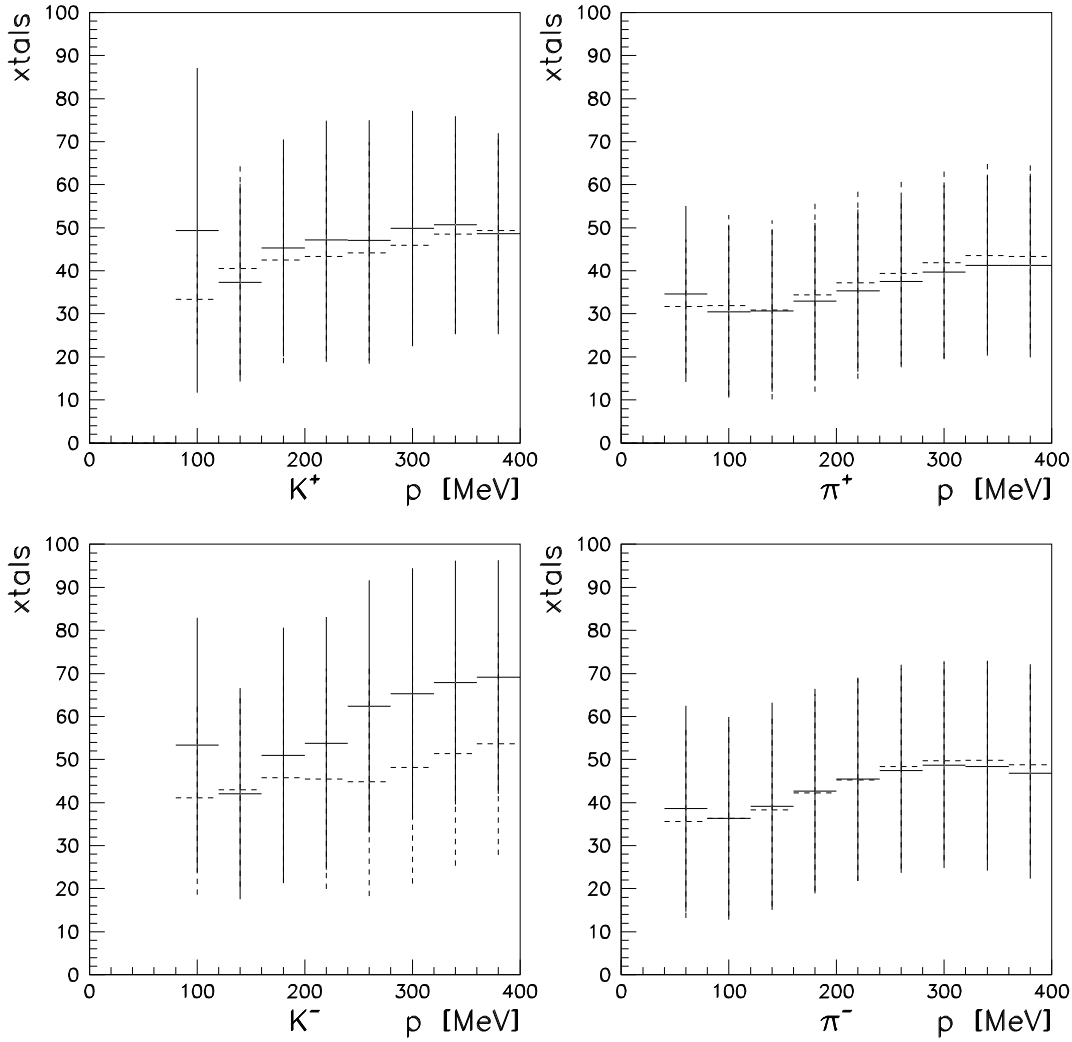

Figure 9: Mean number of crystals examined by TAXI as function of momentum. Monte Carlo (dashed) , data (solid). The error bars indicate the RMS of the distribution.

struct them as a two prong event with the K_L non-interacting (probability about 50%) (see [3]). At the $K\bar{K}$ threshold the K_L and the K^- (K^+) both have the same momentum recoiling against the π. This increases the probability for an interacting K_L to hide inside the charged cluster. In consequence the $a_0(980)$ is enhanced, in the worst case by the amount of the interaction probability. Since the $a_0(980)$ is well separated from other features in this Dalitz plot and it still gives a sharp peak one can correct and analyze it rather independendly.

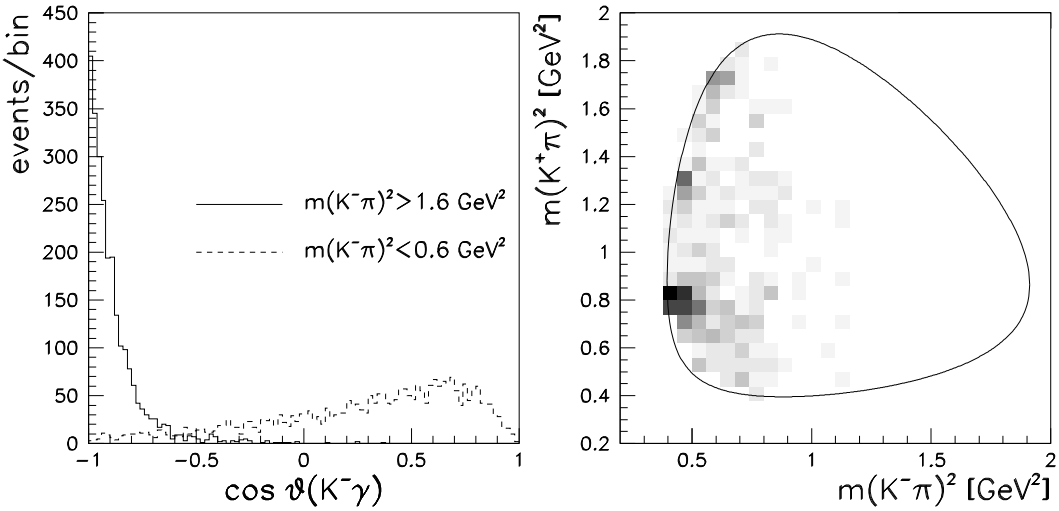

Figure 10: Track-photon correlation for $K^+K^-\pi^0$. *left*: cosine theta between K^- and γ; solid: $p_{K^-} < 400$ MeV/c, dashed: $p_{K^-} > 600$ MeV/c. *Right*: Dalitz plot for events with $K^- - \gamma$ cosine opening angle > 0.7.

8 Split-off Probability

Another systematic to be checked is the probability of mis-identifying a split-off from a charged track with a golden gamma. Since the number of real golden gammas goes to zero close to the matching angle region of 12 degrees, the background is not at all constant. Methods based on the kinematic fit cannot be applied, because this requires all charged particles being already identified, which possible for momenta below 400 MeV/c only. This leaves an extremely small phase space for $\bar{K}K\pi$ channels, and hence the available statistics is not enough for a study of the effect. A qualitative check of the reliability of our golden gamma cut and its Monte Carlo simulation is to compare the opening angle between each PED and the golden track's barrel entrance for positive and negative kaons. We use the channel $K^+K^-\pi^0$. After the selection of two golden gammas the differences between both types of particles vanish in the $\cos\theta$ distribution of *all* PEDs, as can be seen in fig. 11. The larger K^- clusters in real data are sufficiently compact, and there is no evidence yet for abundand extra golden split-offs from the K^- capture and hypernuclei decays.

9 Correction of the $K^+K^-\pi^0$ Dalitz Plot

The acceptance correction based on the CBGEANT Monte Carlo simulation is already applied to the Dalitz plot. We define Dalitz plot asymmetry in terms of

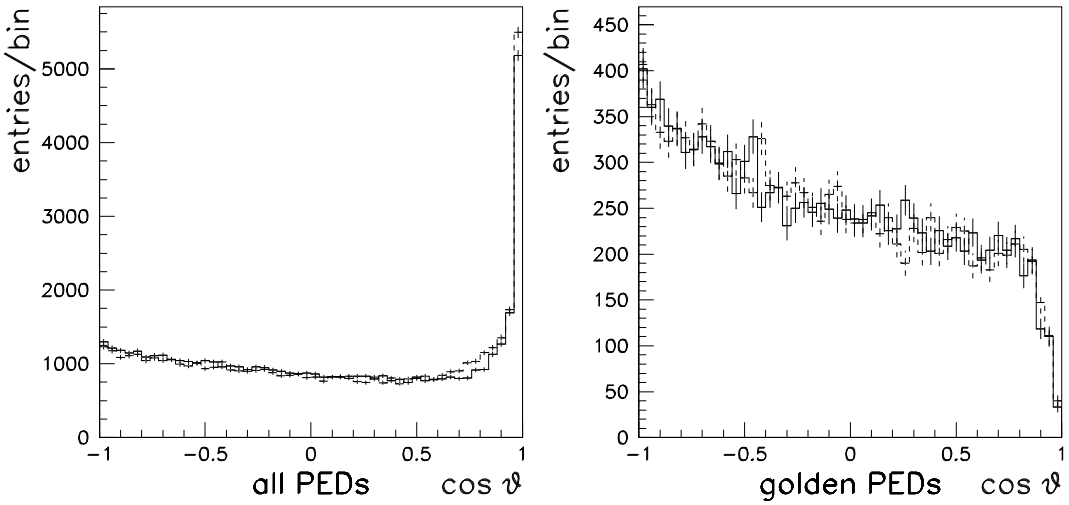

Figure 11: PED-track angular distribution, *left*: all PED's reconstructed, *right*: all golden PED's. θ is the angle between the track entrance in the barrel and the center of each PED found in the event. K^+ solid, K^- dashed.

a χ^2 :

$$\chi^2_{asym} = \sum_{i,j=1}^{n} \frac{(n_{ij} - n_{ji})^2}{\sigma ij^2 + \sigma ji^2}, \tag{5}$$

where n_{ij} is the acceptance corrected number of entries in bin $(ij; i > j)$ of the Dalitz plot and σ_{ij} is the error of n_{ij}. Hence, we compare the population of the upper half with that of the lower half of the phasespace. After normal acceptance correction we obtain an overall $\chi^2_{asym}/bin = 1.210$.

We now correct for the low momentum K^+ acceptance using the eqn.(3) determined in the section matching probability. It applies to low momentum kaons. The error in each bin of the Dalitz plot is scaled simultaneously.

We concentrate in the next step on the K^*-bands to extract the remaining difference in the K^+ versus the K^- acceptance directly from the Dalitz plot. The result is a momentum dependend relative K^+K^- correction, which we compare with the effects already discussed. Figure 12 shows the $K^+K^-\pi^0$ Dalitz plot. The band-areas are marked by lines in the upper left plot. Each band is projected into the opposite $K\pi$ subsystem (see fig. 12 upper right). The projection of the K^{*+} band is divided by the projection of the K^{*-} band. The ratio versus the $K\pi$ invariant mass squared is shown in fig. 12 lower left. In the region 0.6 GeV^2 $< m^2(K\pi) <$ 1.4 GeV^2 the asymmetry ratio is 1. The deviation from 1 in the regions below and above can be understood the following.

In the region below 0.6 GeV^2 the photon blindness is the dominant effect: The π^0 hides more easily under a K^- than under a K^+. The preferred kinematic constellation is a small opening angle between the charged kaon and the π^0. The

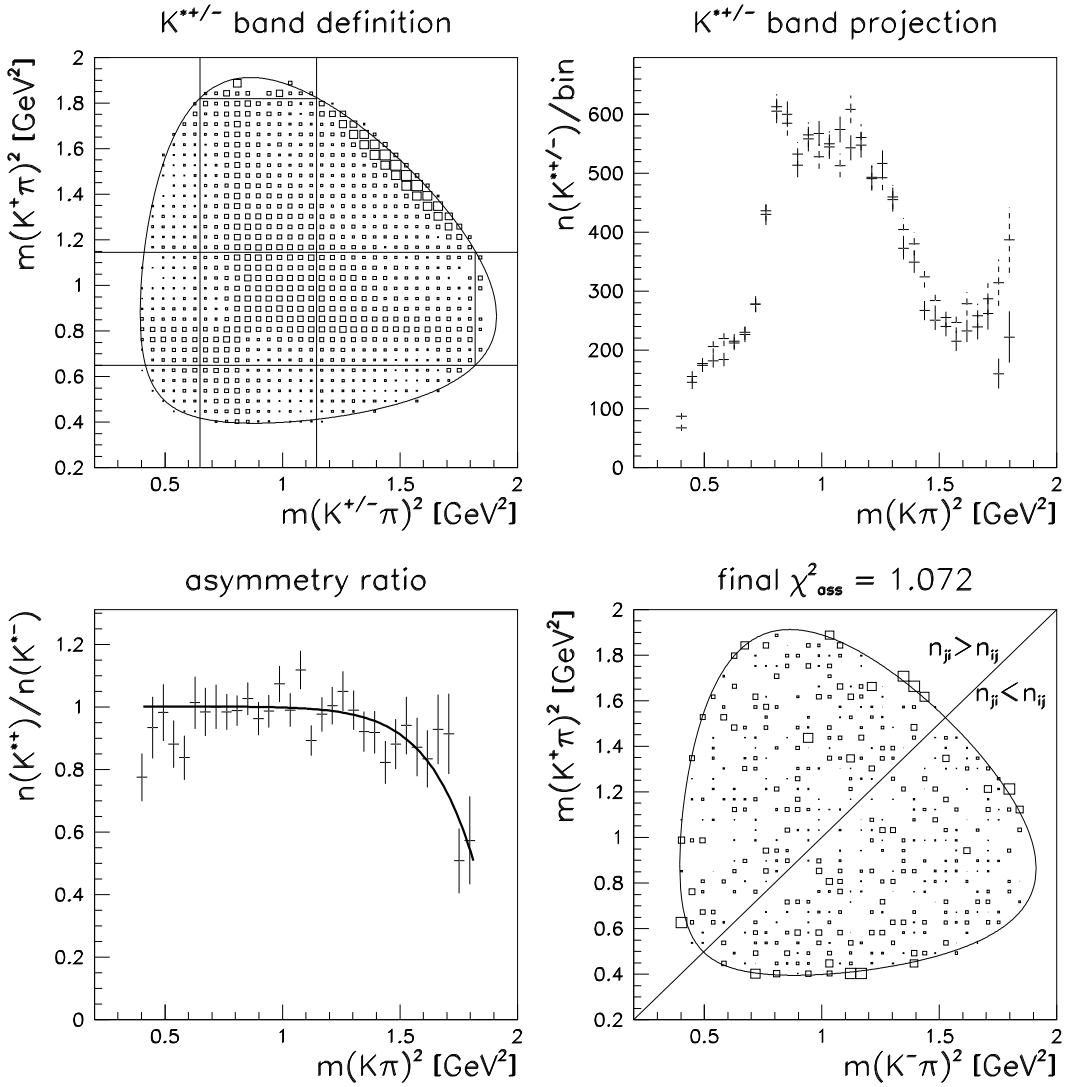

Figure 12:
Upper left: Definition of the K^*-bands in the acceptance corrected plot.
Upper right: Projections of the K^*-bands K^{*+} solid, K^{*-} dashed error bars.
Lower left: Asymmetry ratio as determined from dividing the two $K^\star$ bands; the correction function f_{K^-} is superimposed.
Lower right: asymmetry χ^2 after applying the corrections on the Dalitz plot. *upper left triangle*: $n_{ij} < n_{ji}$, *lower right triangle*: $n_{ij} > n_{ji}$, $(i > j)$

situation occurs in the lower left corner of the Dalitz plot fig.12. An excess of events in the region $m^2 < 0.6$ GeV^2 for K^+ relative to K^- means a ratio lower than 1. However, this deviation is rather small. The second region above 1.4 GeV^2 shows strong systematic differences. The effects from unmatched golden tracks call for the drop in the ratio at 1.75 GeV^2.

We use the following parametrisation to be adjusted to the asymmetry ratio :

$$f_{K^-} = a_1 \cdot \{1 - a_2 \cdot \exp\left(-\frac{m^2_{K^-\pi} - a_3}{a_4}\right)\}, \qquad (6)$$

with

a_1 : 1.00 ± 0.03

a_2 : 3.68 ± 0.08

a_3 : 0.86 ± 0.20

a_4 : 54.83 ± 20.00

It is shown in fig. 12, lower left corner. We multiply entries and errors of the K^+ acceptance corrected Dalitz plot bins with the function f_{K^-} eqn. (6). The final χ^2 distribution of the corrected Dalitz plot is shown in fig. 12 for both positive and negative differences. After application of all the corrections the asymmetry test gives now $\chi^2_{asym}/bin = 1.072$ in $K^+K^-\pi^0$. We have achieved a rather symmetric $K^+K^-\pi^0$ Dalitz plot.

10 Correction of the $K_L K^{\pm}\pi^{\mp}$ Dalitz Plot

We use the same procedure to extract the relative behaviour from the two $K^{\pm}K_L\pi^{\mp}$ Dalitz plots as in the previous section. The statistics for that investigation is lower than that from $K^+K^-\pi^0$. The $K^{\star\pm}$ bands were defined the same in the different plots. Only the low momentum K^+ correction needs to be done. The quotient $K^{\star-}/K^{\star+}$ is shown in fig. 13. One observes the same declination as in $K^+K^-\pi^0$. We adopt the function f_{K^-} eqn. (6) which is superimposed in fig. 13. The curve describes the data with a probability of 41% . The correction is used to prepare the two Dalitz plots [3].

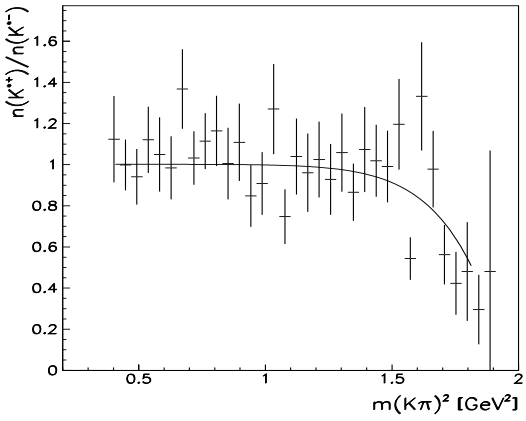

Figure 13:
The ratio $K^{\star-}/K^{\star+}$ extracted from $K_L K^+\pi^-$ and $K_L K^-\pi^+$. Superimposed is the identical function as for $K^+K^-\pi^0$.

11 Summary and Discussion of the Results

We have listed the main points of the K^- systematics which need to be taken into account as further acceptance corrections in comparison to the K^+. The global correction amounts to about 5% . The application of momentum dependend corrections yields a symmetric $K^+K^-\pi^0$ Dalitz plot and adjusts $K_L K^-\ \pi^+$ to $K_L K^+\ \pi^-$.

References

[1] S.Ravndal and M.Goossens, GEANT, Detector description ans simulation tool, CERN Program library long writeup W5013

[2] M.Benayoun et al., Split-off recognition in data with charged tracks. The TAXI logics, CB-Note 280 (1995)

[3] M.Heinzelmann, S.Spanier,
Analysis of $K^\pm K_L \pi^\mp$ in $\bar{p}\pi$annihilation at rest, CB-Note